CERN
CH 1211 Geneva 23
Switzerland

EST Division

Group Reference.: **EST-ME/AB/fgm**
EDMS No.: **457138**

Technical Note
EST-ME/2003-006

AN ANALYTICAL MODEL TO STUDY TRANSIENT THERMAL STRESSES IN GRAPHITE TARGET RODS HIT BY OFF-AXIS BEAM FOR CNGS FACILITY

Alessandro Bertarelli

Abstract

An analytical method to determine the transient stresses induced by a fast extracted proton beam hitting off-axis a graphite rod was fully developed. An exact solution for the temperature field was first determined, by means of Fourier-Bessel expansions Quasi-static thermal stresses were then computed as a function of the calculated temperature distribution, making use of Goodier's method for the thermoelastic problem. Finally, the contribution of dynamic stresses due to longitudinal and bending waves was also determined by using mode-summation modal analysis.

Keywords: Thermal stresses, Target rods, transient analysis, CNGS

July 2003

Distribution: See list
Secretariat: EST-ME/*F. Girard-Madoux*

Table of Contents

List of figures

1. INTRODUCTION

The CNGS project consists in producing a neutrino beam at CERN and sending it towards the Gran Sasso INFN laboratory. A beam of this type is generated from collisions of protons in a beam with protons and neutrons in graphite target, focussing the particles produced (pions and kaons in particular – secondary particles neutrino parent) in the desired direction (Figure 1-1).

A 400 GeV proton beam will be extracted from the SPS accelerator. This proton beam will hit a target a few meters downstream from the extraction point (BA4).

The CNGS target will consist of a series of small graphite cylinders[1]. The size of the target has been chosen so that it will provide as many secondary particles as possible. The graphite rods must absorb the great heat and thermo-mechanical shock due to the energy deposited by the proton beam; the target must therefore be cooled with a jet of high-pressure helium gas in a closed circuit.

The particles produced in the target then enter a system of magnetic horns, which will focus positive particles with a mean energy of 35 GeV and defocus the negative particles.

The target should be dimensioned such that almost all incident protons interact but, at the same time, cause as little absorption or scattering of the secondary particles as possible.

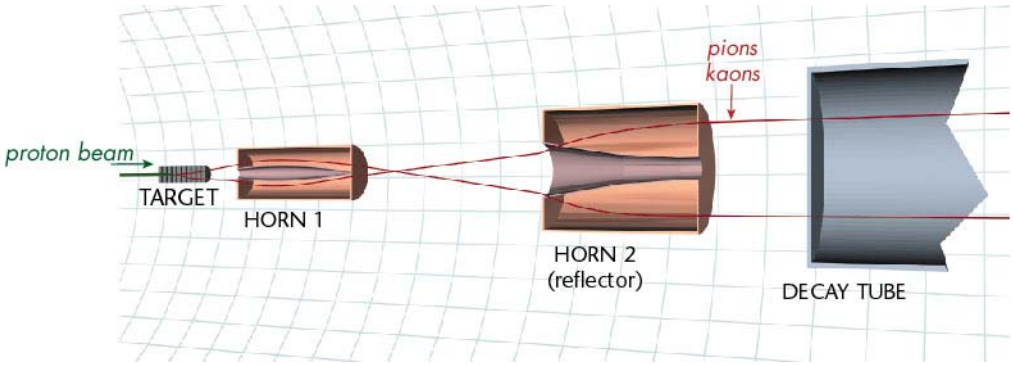

Figure 1-1 CNGS secondary particle production scheme

2. TARGET MAIN PARAMETRES

Every graphite rod is simply supported at the extremities and has the following geometrical dimensions:

Radius: $R = 2.5\ mm$

Length: $L = 100\ mm$

Each rod is submitted to a high intensity series of proton "pulses". Each pulse lasts 10 microseconds and its power density is constant over such a time. Pulses are emitted with a period of 50 milliseconds.

The energy deposited by the beam has a Gaussian distribution over the rod section and is supposed constant over the length. The beam is eccentric with respect to the rod axis. We

[1] In a cast aluminium target container 11 rods of graphite, 10 cm long and 5mm in diameter each, form a 2m long target array.

assume here the eccentricity η is positive when measured downward on the vertical y-axis (θ=270°)

Extraction time: $t_{sp} = 10\mu s$

Extraction cycle period: $t_b = 50\ ms$

Number of incident protons: $N_p = 3.5 \cdot 10^{13}\ prot$

Maximum energy density: $E_{dMax} = 245.991 \frac{J}{kg \cdot 10^{10}\ prot}$

Energy density standard deviation: $\sigma = 0.63\ mm$

Specific energy $U(r,\theta) = E_d(r,\theta) \cdot N_p \times 10^{10}$

Maximum specific energy $U_{\max} = 8.61 \times 10^5 \frac{J}{kg}$

Beam eccentricity (w.r.t. rod axis) $\eta = 0 \div 1.5 mm$

Graphite density: $\rho = 1850 \frac{kg}{m^3}$

Maximum power density $W_{Max} = U_{Max} \frac{\rho}{t_s} = 1.593 \cdot 10^{14} \frac{W}{m^3}$

The thermodynamic and mechanical properties of graphite are temperature dependent. Anyhow, to simplify our analytical approach, we assume these properties to be constant over temperature:

Mean specific heat $c_m = 1350 \frac{J}{kg \cdot K}$

Mean thermal conductivity $k_m = 70 \frac{W}{m \cdot K}$

Mean coefficient of thermal expansion: $\alpha_m = 3.9 \cdot 10^{-6} \frac{1}{K}$

Mean Young's Modulus: $E = 10.49 GPa$

Poisson's ratio: $\nu = 0.15$

Initial uniform temperature is 20°C. However, for sake of simplicity, as main parameters are supposed independent of temperature, we assume initial zero temperature. Real temperatures can be computed by offsetting values by 20°C.

3. TEMPERATURE DISTRIBUTION

3.1 Introduction

We want to calculate the exact temperature distribution for a non-uniform off-axis heating with Gaussian energy density.

To do so we want to solve the heat conduction equation in cylindrical coordinates.

$$\frac{\partial^2 T}{\partial r^2}+\frac{1}{r}\frac{\partial T}{\partial r}+\frac{1}{r^2}\frac{\partial^2 T}{\partial \theta^2}+\frac{1}{k}\frac{\partial Q}{\partial t}=\frac{1}{\kappa}\frac{\partial T}{\partial t} \quad \textbf{(1)}$$

where Q is the thermal energy contained in the reference volume and

$$\kappa=\frac{k_m}{c_m\rho} \quad \textbf{(2)}$$

is the *thermal diffusivity.*

In the axisymmetric case, equation (1) can be simplified by dropping the θ variable (T is independent of the angle θ), leading to a simpler problem [7]. Unfortunately, because of eccentricity, for this case both r and θ must be retained. As we are interested in temperature distribution after the first pulse, when heat is no longer generated inside the cylinder, the term in Q disappears. Equation (1) then reduces to the following diffusion problem:

$$\frac{\partial^2 T(r,\theta,t)}{\partial r^2}+\frac{1}{r}\frac{\partial T(r,\theta,t)}{\partial r}+\frac{1}{r^2}\frac{\partial^2 T(r,\theta,t)}{\partial \theta^2}=\frac{1}{\kappa}\frac{\partial T(r,\theta,t)}{\partial t} \quad \textbf{(3)}$$

Terms in z are not appearing having supposed that temperature distribution is constant along rod axis.

Having assumed that the Maximum energy density (burst "centre") lies at $r=\eta$, $\theta=3\pi/2$, the specific energy takes on the following expression:

$$U(r,\theta)=U_{Max}e^{-\frac{r^2+\eta^2+2r\eta\sin\theta}{2\sigma^2}} \quad \textbf{(4)}$$

3.2 Initial and boundary conditions

Assuming no heat diffusion process takes place during the extraction time, the initial[2] temperature distribution is given by:

$$T(r,\theta,0)=T_0(r,\theta)=\frac{U(r,\theta)}{c_m} \quad \textbf{(5)}$$

Maximum temperature can be immediately calculated:

$$T_{0Max}=\frac{U_{Max}}{c_m}=637.8^{\circ}C \quad \textbf{(6)}$$

[2] We assume here that time t=0 corresponds to the end of the extraction time. This assumption will be modified for the dynamic analysis.

The boundary condition stems from the hypothesis of adiabatism, which can be retained since time constants for this phenomenon are very short.

$$\frac{\partial T(R,\theta,t)}{\partial r} = 0 \quad \textbf{(7)}$$

Equation (7) states that the temperature gradient on the outer surface is zero, as required by the adiabatic hypothesis.

The problem would be dramatically simplified if we could separate the three problem variables: *r, θ, t*. To do so, we replace the initial temperature distribution given by eq.(5), with its Fourier-series expansion:

$$T_0(r,\theta) = \sum_{k=0}^{\infty} a_{2k} \cos 2k\theta + a_{2k+1} \sin(2k+1)\theta = \sum_{n=0}^{\infty} a_n(r) H_n(\theta) \quad \textbf{(8)}$$

where a_n are the expansion coefficients, function of *r*. Only even terms are present in the series since temperature distribution is symmetric with respect to y-axis. For our analysis, the series can be truncated. It can be shown that 8 terms (k_{Max}=3, n_{Max}=7) are sufficient to closely reproduce a gaussian distribution.

3.3 Thermal analysis

Thanks to previous assumptions, we may assume that the function *T(r, θ, t)* can be reduced to the following form:

$$T(r,\theta,t) = \sum_{n} F_n(r) \cdot G_n(t) \cdot H_n(\theta) \quad \textbf{(9)}$$

Where H_n is the harmonic term defined in equation (8):

Expression (9) must satisfy diffusion equation (3).

Making use of separation of variable method, we can obtain a solution of the following form [1]:

$$T(r,\theta,t) = \sum_{n} \sum_{s} C_{n,s} J_n(\lambda_{n,s} r) \cdot e^{-\kappa \cdot \lambda_{n,s}^2 \cdot t} \cdot H_n(\theta) \quad \textbf{(10)}$$

where J_n is a Bessel function of the first kind of order n, $C_{n,s}$ are numerical coefficients obtained from the initial condition (5) and $\lambda_{n,s}$ are the eigenvalues of the problem obtained by the application of the adiabatic condition (7).

3.4 Results

The thermal analysis has shown several important aspects:

1. Final uniform temperature slightly decreases when the eccentricity is increased. Assuming initial temperature is 0, final temperature is *81ºC* for *η=0* and *74.7ºC* for *η=1.5mm*. This is due to the higher energy lost when eccentricity augments.
2. The time necessary to reach thermal equilibrium significantly rises with eccentricity (Figure 3-2). For *η=0*, the time to reach a maximum temperature

gradient of 1ºC is *0.093s* while for η*=1.5mm* it becomes ***0.364s***, i.e. 4 times as much. The rate of increase of this time is initially very sharp, and for η*=0.5mm*, it is already *0.292s*.

3. Given the time necessary to reach thermal equilibrium, the effects of one burst have not waned when next one takes place. Since thermodynamic and mechanical parameters are supposed constant, one can compute thermal field by simple superposition

As one could expect, when eccentricity is zero, these results perfectly match those obtained for the axially symmetric study [7].

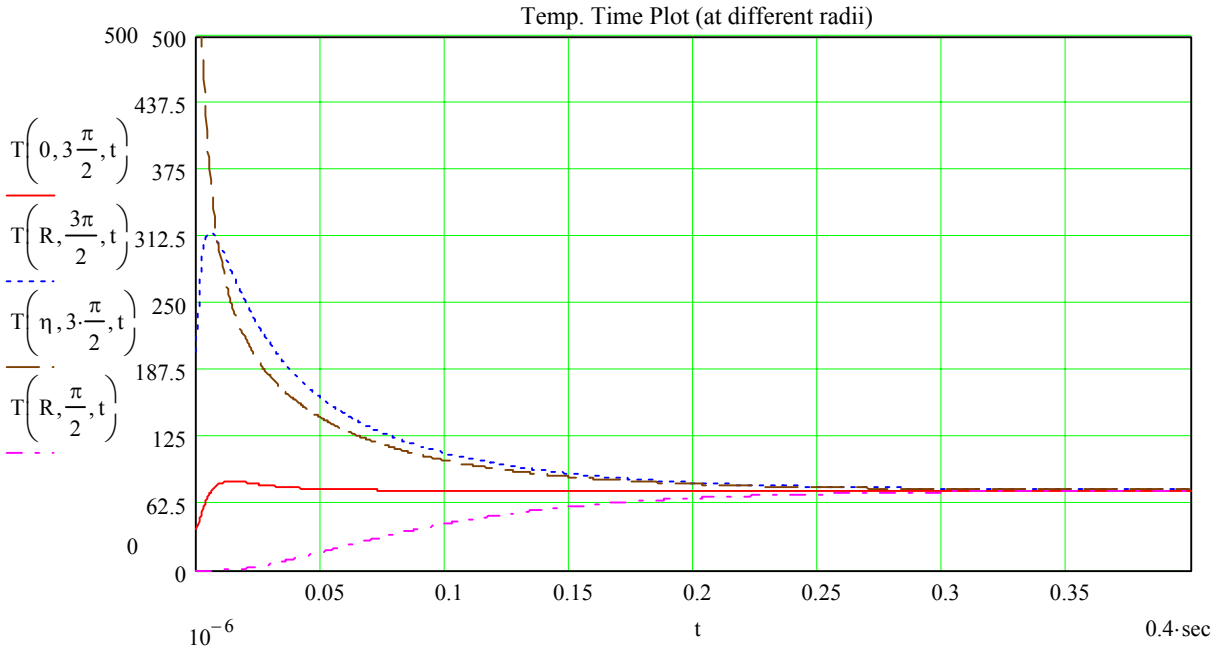

Figure 3-1 Temperature distribution as a function of time (η=1.5mm)

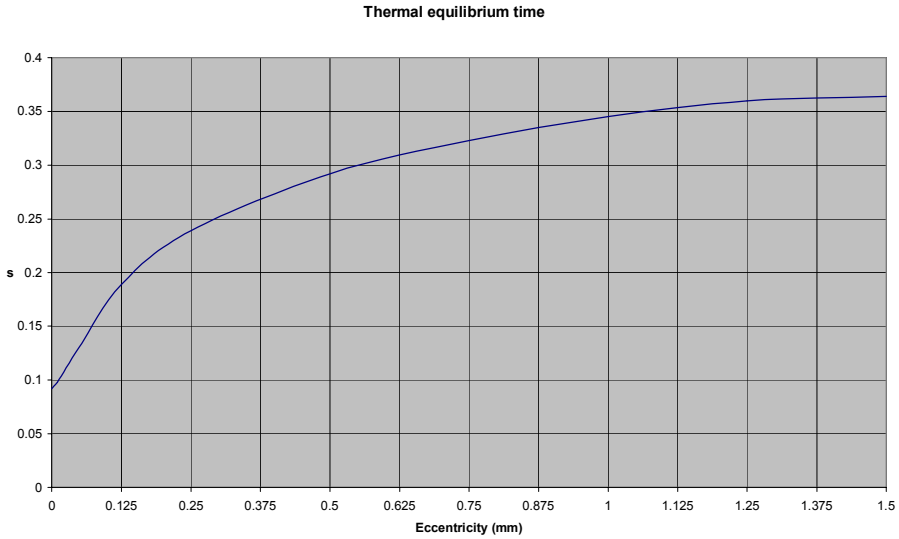

Figure 3-2 Time required to reach thermal equilibrium (ΔT≤1ºC) as a function of eccentricity

4. QUASI-STATIC STRESSES

4.1 Introduction

Calculation of quasi-static stresses is not as straightforward as it is in the case of axisymmetric distribution [7]. One possible approach is to make use of Goodier's method [2], [3] applied to the plain-strain case (hypothesis of a long cylinder). According to this method, stress components are calculated from the superposition of two effects: 1) stresses arising from the application of a *displacement potential* $\psi(r,\theta,t)$ which satisfies the thermoelastic equation, but not the mechanical boundary conditions (free-boundary), 2) stresses due to isothermal pressure loads applied on the outer surface to restore the free-boundary condition.

It can be shown that, in the case of pure heat conduction, the general thermoelastic equation is automatically satisfied if the displacement potential ψ is a solution of the following equation:

$$\frac{\partial \psi}{\partial t} = \frac{1+\nu}{1-\nu}\alpha\kappa T \tag{11}$$

where α is coefficient of thermal expansion.

Since T becomes uniform for $t \to \infty$, ψ can be immediately calculated:

$$\psi(r,\theta,t) = -\frac{1+\nu}{1-\nu}\alpha\sum_n\sum_s \frac{C_{n,s}J_n(\lambda_{n,s}r)\cdot e^{-\kappa\cdot\lambda_{n,s}^{\ 2}\cdot t}}{\lambda_{n,s}^{\ 2}} H_n(\theta) + A \tag{12}$$

where A is a generic constant of integration, not affecting the displacement field.

Once ψ is known, plane displacements components in radial and tangential direction, deriving from this potential, $\overline{u'}$ and $\overline{v'}$[3] can be easily found by means of the following relations:

$$\begin{aligned} \overline{u'} &= \frac{\partial \psi}{\partial r} \\ \overline{v'} &= \frac{1}{r}\frac{\partial \psi}{\partial \theta} \end{aligned} \tag{13}$$

Subsequently, strain and stress components, $\overline{\sigma'_r}, \overline{\sigma'_\theta}$, $\overline{\tau'_{r\theta}}$ and $\overline{\sigma'_z}$, can be calculated from general cinematic relations for two-dimensional problems and Hooke's general law when $\varepsilon_z=0$ [2]:

$$\begin{aligned} \overline{\varepsilon'_r} &= \frac{\partial \overline{u'}}{\partial r} \\ \overline{\varepsilon'_\theta} &= \frac{\overline{u'}}{r} + \frac{1}{r}\frac{\partial \overline{v'}}{\partial \theta} \\ \overline{\gamma'_{r\theta}} &= \frac{1}{r}\frac{\partial \overline{u'}}{\partial \theta} + \frac{\partial \overline{v'}}{\partial r} - \frac{\overline{v'}}{r} \end{aligned} \tag{14}$$

[3] The axial component is zero according to the initial plain-strain hypothesis.

$$
\begin{aligned}
&\overline{\sigma'_r} - \nu\left(\overline{\sigma'_\theta} + \overline{\sigma'_z}\right) = E\left(\overline{\varepsilon'_r} - \alpha T\right)\\
&\overline{\sigma'_\theta} - \nu\left(\overline{\sigma'_r} + \overline{\sigma'_z}\right) = E\left(\overline{\varepsilon'_\theta} - \alpha T\right)\\
&\overline{\sigma'_z} - \nu\left(\overline{\sigma'_r} + \overline{\sigma'_\theta}\right) = -E\alpha T\\
&\overline{\tau'_{r\theta}} = G\overline{\gamma'_{r\theta}}
\end{aligned}
\qquad \textbf{(15)}
$$

As mentioned above, the stress distribution calculated from the displacement potential satisfies the thermoelastic equation, but not the boundary condition, requiring zero-forces on the external surface. Invoking the principle of superposition, we now add a pressure field removing non-zero forces on the rod surface, thus restoring the correct boundary conditions. To do so, we make use of the *Michell's* formulation of the *Airy stress function $\phi(r,\theta,t)$* in polar coordinates, applied to an ordinary plain-strain problem [2]. Once $\phi(r,\theta,t)$ is known, stress components $\overline{\sigma''_r}, \overline{\sigma''_\theta}$, and $\overline{\tau''_{r\theta}}$ can be calculated from the following expressions:

$$
\begin{aligned}
&\overline{\sigma''_r} = \frac{1}{r}\frac{\partial\phi}{\partial r} + \frac{1}{r^2}\frac{\partial^2\phi}{\partial\theta^2}\\
&\overline{\sigma''_\theta} = \frac{\partial^2\phi}{\partial r^2}\\
&\overline{\tau''_{r\theta}} = -\frac{\partial}{\partial r}\left(\frac{1}{r}\frac{\partial\phi}{\partial\theta}\right)
\end{aligned}
\qquad \textbf{(16)}
$$

4.2 Quasi-static stresses for zero-axial strain

By superposing stress components obtained from previous method, we find quasi-static stresses. Previous calculations were made in the initial hypothesis of zero-axial strain: the resulting axial stress $\overline{\sigma}_{z0}$ corresponds to the case of a rod restrained by two plates at the extremities preventing any axial deformation. So we obtain:

$$
\begin{aligned}
&\overline{\sigma_r} = \overline{\sigma'_r} + \overline{\sigma''_r}\\
&\overline{\sigma_\theta} = \overline{\sigma'_\theta} + \overline{\sigma''_\theta}\\
&\overline{\tau_{r\theta}} = \overline{\tau'_{r\theta}} + \overline{\tau''_{r\theta}}\\
&\overline{\sigma_{z0}} = \nu\left(\overline{\sigma_r} + \overline{\sigma_\theta}\right) - E\alpha T
\end{aligned}
\qquad \textbf{(17)}
$$

Results for the stresses at most relevant locations for η=*1.5mm* and for t= t_{sp} are given in the following graphs.

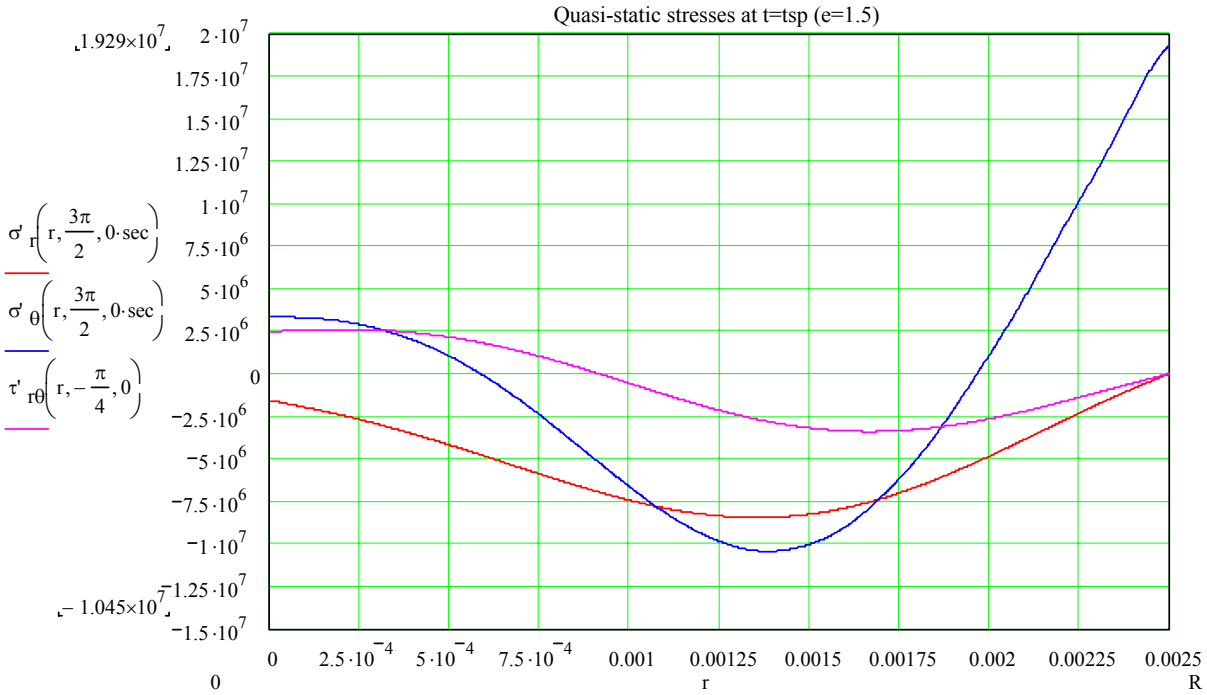

Figure 4-1 In-plane quasi-static stresses as a function of radius at $t=t_{sp}$

Figure 4-2 Axial stress at zero-strain as a function of radius (η=1.5mm)

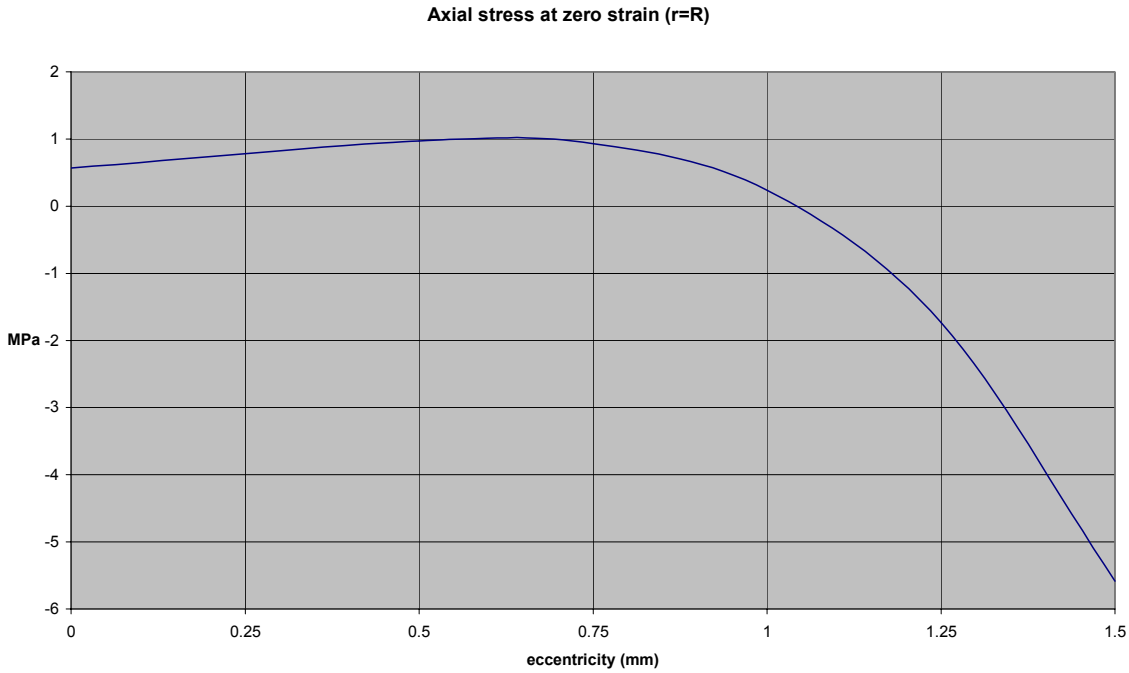

Figure 4-3 Axial stress at position r=R, θ=3π/2 as a function of eccentricity

The analysis of quasi-static stresses with zero-axial strain leads to the following conclusions:

1. Polar shear stress is non zero when eccentricity is present.
2. Maximum negative tangential stress is found for $r \approx 0.9\eta$, while maximum negative radial stress is found for $r \approx 0.93\eta$. Tangential stress is slightly more than radial stress in magnitude when $\eta > 0$. Both values decrease in magnitude when η augments
   (for $\eta = 0\ \sigma_\theta = \sigma_r = -13.4MPa$; for $\eta = 1.5\text{mm}\ \sigma_\theta = -10.44MPa$
   and $\sigma_r = -8.46MPa$)
3. Maximum positive tangential stress is found for $r=R$. Its values varies from 3.88 MPa for $\eta=0$ up to 19.5 MPa for $\eta=1.5mm$.
4. Shear stress is zero on the symmetry plane, while has its maximum for $\theta \approx -45°$.
5. Axial stress for zero-axial strain at $r=R$ is minimum for $\eta=1.5$, it then increases rapidly for η down to 1mm and thereafter becomes more stable, with a maximum of around 1MPa for $\eta=0.6mm$ (Figure 4-2)

4.3 Total quasi-static axial stress

Axial stress in previous calculations was obtained in the hypothesis of zero axial strain. In reality the rods are free at their extremities: to restore such condition we have to ensure that the axial force and bending moment resulting from axial stress at each section of the rod are zero.

In order to do so, we first calculate resultant axial force and moment for the previous configuration and then superimpose at the extremities the same force and moment changed in

sign. Resulting axial stress will be the actual longitudinal stress acting on the free rod far from the extremities[4].

Equivalent axial force in the case of restrained rod (zero-strain) is calculated via the following integral:

$$F_z = -2\int_{-\frac{\pi}{2}}^{\frac{\pi}{2}}\int_0^R \overline{\sigma_{z0}} r dr d\theta \quad \textbf{(18)}$$

It is very interesting to note that *Fz* remains constant over the time for $t>t_{sp}$. For $\eta=0mm$, its value exactly matches the one calculated for the axisymmetric case [7]. It can be shown that for the off-axis as well as for the axisymmetric case, the resultant axial force is proportional to the total deposited energy or, in other words, to the final temperature:

$$F_z = E\alpha T_{fin}\pi R^2 \quad \textbf{(19)}$$

The value of *Fz* slightly diminishes with increasing eccentricity, since deposited energy is less for high eccentricity. For $\eta=0$, $Fz=65N$, while for $\eta=1.5mm$, $Fz=60N$.

The equilibrating bending moment about horizontal axis[5] ($\theta=0^o$) *Mx* can be computed likewise.

$$M_x = -2\int_{-\frac{\pi}{2}}^{\frac{\pi}{2}}\int_0^R \overline{\sigma_{z0}} r^2 \sin\theta dr d\theta \quad \textbf{(20)}$$

In this case the result depends upon time and becomes zero when $t \to \infty$, as one could expect, since temperature gradient disappears. Anyhow, it is interesting to observe that M_x remains substantially constant for the first millisecond (Figure 4-4); this consideration will be very important for the dynamic analysis. It is also interesting to note that the ratio *Mx/Fz* is very close to eccentricity (a bit less).

Total quasi-static axial stress is given by the superposition of $\overline{\sigma}_{z0}$ with the axial stresses generated by F_z and M_x.

$$\overline{\sigma}_z = \overline{\sigma}_{z0} + \frac{F_z}{\pi R^2} + \frac{Mx \cdot r\sin\theta}{\frac{\pi R^4}{4}} \quad \textbf{(21)}$$

Resulting stress is given in Figure 4-5.

[4] At the two rod extremities this solution will not be strictly applicable. Anyhow, for the sake of results, this is not too worrisome since, as we will see, the most critical section is found at mid-rod where the method is largely valid.
[5] The bending moment about the vertical axis is always zero because of symmetry.

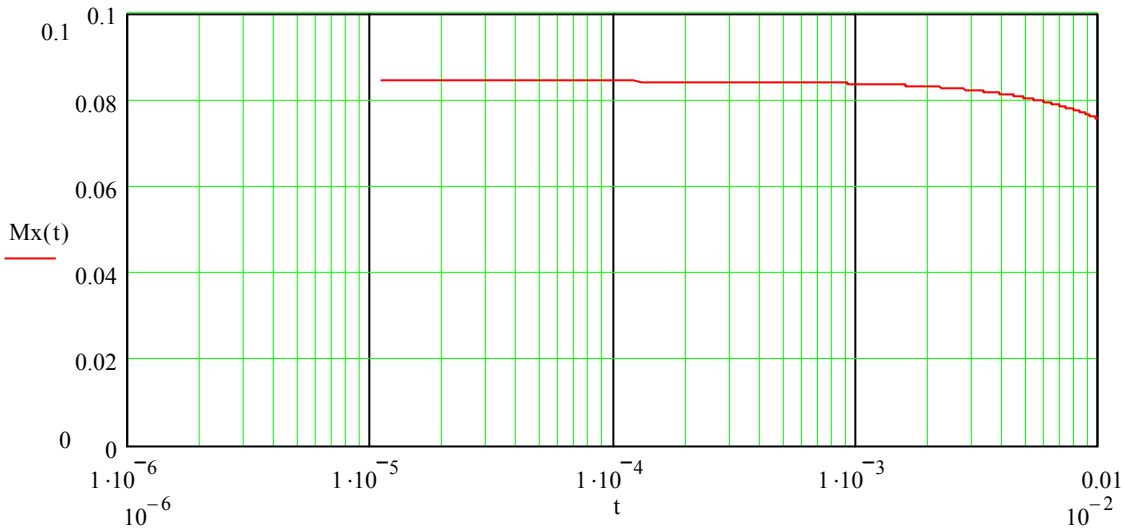

Figure 4-4 Bending moment about x-axis as a function of time (η=1.5mm)

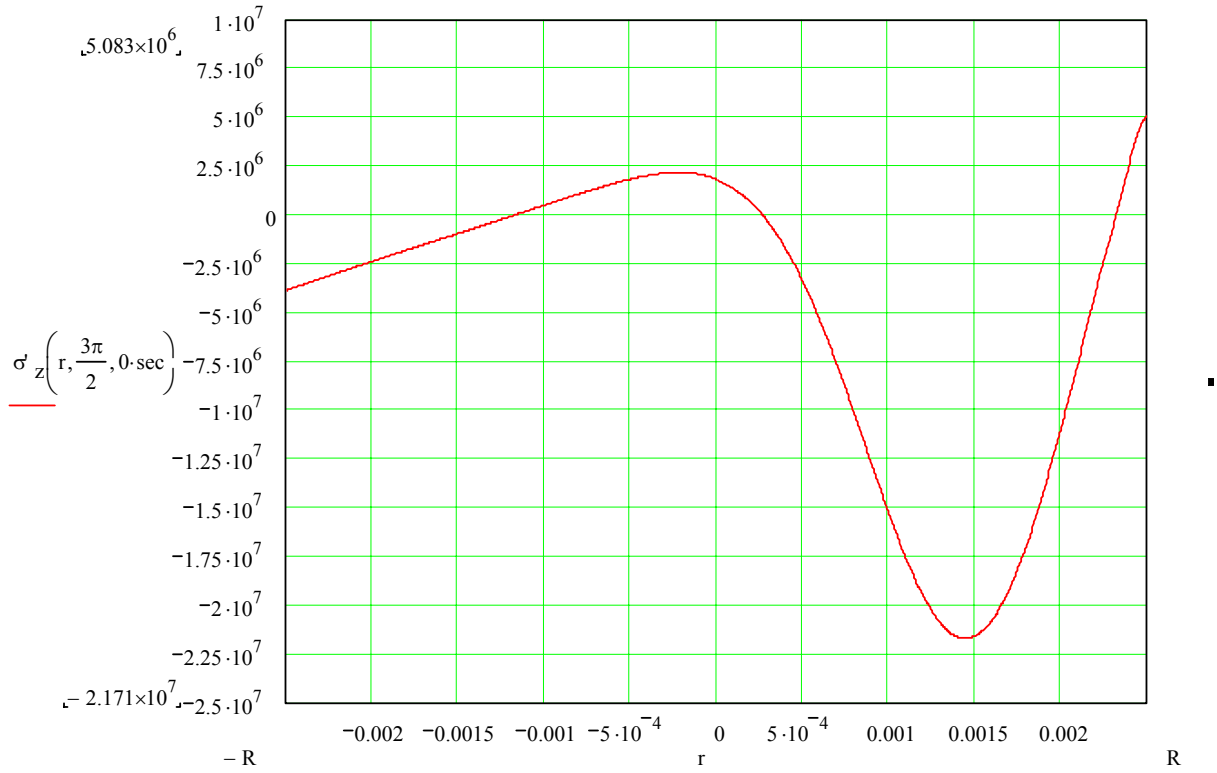

Figure 4-5 Quasi-static axial stress for η=1.5mm

Axial stress has a minimum close to $r=\eta$ and is maximum for $r=R$. Minimum slightly varies with eccentricity (from *-26.8MPa* for $\eta=0$ to *-21.8MPa* for $\eta=1.5mm$) while maximum increases from *3.88MPa* for $\eta=0$ to *5.26MPa* for $\eta=1.5mm$.

5. DYNAMIC STRESSES

5.1 Introduction

In the previous chapter, quasi-static stresses were exactly calculated. However, the effect of inertia was completely neglected. We know from previous analyses [7] that the dynamic effect induced by longitudinal and radial waves is very relevant on the longitudinal stresses, while the contribution of radial waves over in-plane stresses is almost negligible. This assumption is also confirmed by other analytical studies [8]. Therefore we will focus our dynamic analysis on the calculation of longitudinal and bending oscillations while we completely neglect the presence of radial waves.

The approach will be different from what previously used: instead of trying to solve explicitly the equations of motions, we make use of the modal analysis, studying the time response to two constant excitations rising from zero to constant value in t_{sp} (Figure 5-1), represented by the equivalent axial force *Fz* and the bending moment *Mx* applied at the extremities of the rod. This approach can intuitively be justified as follows: from a purely mechanical point of view we can think of our system as an off-axis preloaded spring clamped between two plates which are progressively removed in a time equal to t_{sp}. The removal of the plates will induce in the spring longitudinal and flexural oscillations which can be calculated.

As a matter of fact M_x is not constant after t_{sp}, but as shown in Figure 4-4, it can be considered as such at least for the first $1000\mu s$, which is the time domain of greatest interest for our analysis.

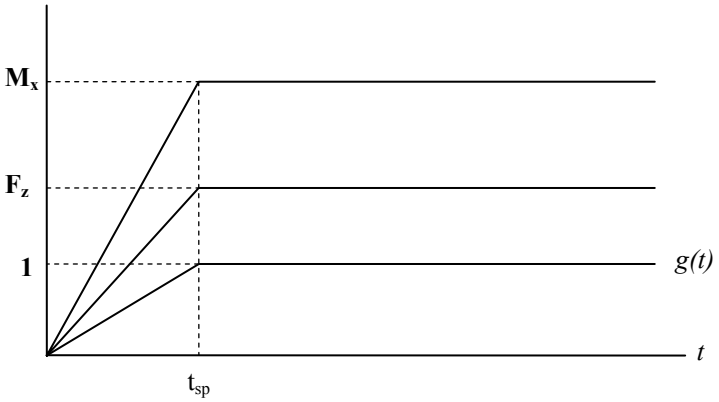

Figure 5-1 Equivalent dynamic excitations (Constant with rise time)

To calculate time-response we make use of the Mode-summation method, which basically expands the deformation in terms of the *normal modes* $\phi_{zi}(z)$ or $\phi_{fi}(z)$ and of the generalized coordinates $q_{zi}(z)$ or $q_{fi}(z)$ of a simply supported uniform beam loaded at the extremities with *Fz(t)* or *Mx(t)* respectively [4].

The equation of motion for each linearly independent mode is obtained by the application of the Lagrange's equation which leads to,

$$\frac{d^2 q_i}{dt^2} + \omega_i{}^2 q_i = \frac{Q_i}{M_i} \tag{22}$$

where M_i and Q_i are the generalized mass and generalized force for the i^{th} mode.

The generalized force Q_i is obtained from the work done by the action F_z or M_x applied at the extremities in the virtual displacement δq_i

5.2 Flexural modal analysis

In case of bending, the lateral displacement of a simply supported beam *w(z,t)* can be expanded in terms of the natural modes and of the generalized coordinates as follows:

(23) $$w(z,t) = \sum_i \phi_{f_i}(z) \cdot q_{f_i}(t)$$

If we apply the bending moment M_x at the rod extremities, with a time history as shown in Figure 5-1, the generalized force for the i^{th} mode takes the following expression:

(24) $$\frac{Q_{f_i}(t)}{M_i} = \frac{Mx(t_{sp})\sqrt{2} \cdot i\pi}{M \cdot L}\left[1-(-1)^i\right] \cdot g(t) = F_{f_i} \cdot g(t)$$

where M is the mass of the rod, and *g(t)* is the unit excitation shown in Figure 5-1.

The expressions of natural (circular) frequencies and mode shapes[6] for a simply supported beam under bending are given by:

(25) $$\phi_{f_i}(z) = \sqrt{2}\sin(\frac{i\pi z}{L})$$

(26) $$\omega_{f_i} = (i\pi)^2\sqrt{\frac{EJ}{ML^3}}$$

where J is the moment of inertia of the rod circular section. The fundamental frequency and period of the system are given by:

$$\frac{\omega_{f_1}}{2\pi} = 467.5Hz$$

$$T_{f_1} = 2.139 \cdot 10^{-3} s$$

The solution of equation (22) as a function of F_{fi} is known when an excitation *g(t)* is applied [4].

The calculation of the dynamic bending stress induced by lateral displacement *w(z,t)* immediately follows and is given by:

(27) $$\sigma_{zDyn}(r,\theta,z,t) = Ew''(z,t) \cdot r\sin\theta$$

where $w''(z,t)$ is the second derivative of the lateral displacement w.r.t. *z*.

---

[6] Strictly speaking, the use of these mode shapes leads to a curvature $w''(z,t)$ which is always zero at the extremities and does not satisfy the boundary condition Mx(t)=EJ $\boldsymbol{w''(0,t)}$. Nonetheless we retain this approach since we know that the solution is not valid at the extremities and the value of EJ $w''(z,t)$ approaches Mx when *z→0* or *z→L* (see Figure 5-3). The same goes for the longitudinal dynamic stress.

In the following graphs results are given for $\eta=1.5mm$, approximating equation (23) with the first 60 terms of the expansion.

It is interesting to note that, in line with the fundamental period, the first bending stress peak is reached roughly after *1ms*, i.e. slightly less than the first half-period. Its value for $r=R$ is *19.6MPa* (Figure 5-6).

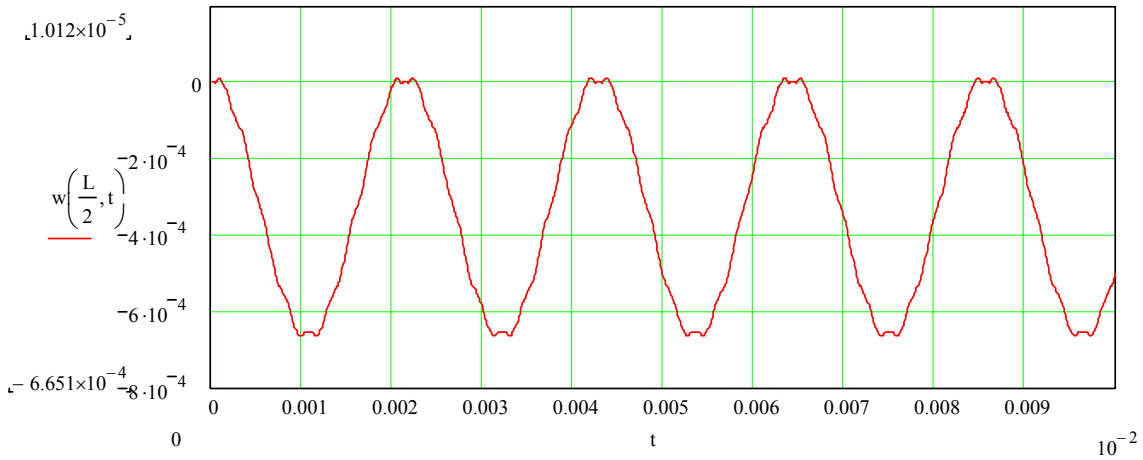

Figure 5-2 Lateral displacement at mid rod as a function of time (η=1.5mm)

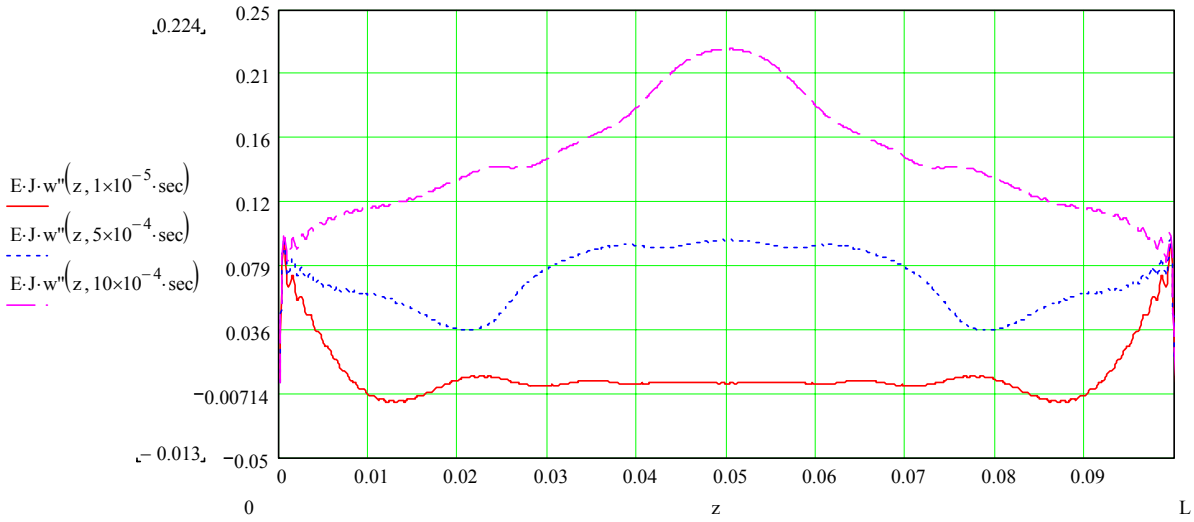

Figure 5-3 Equivalent moment EJw" along the rod at different instants (η=1.5mm)

Figure 5-4 is very interesting since it shows that the highest bending moment is found at the rod centre, it slightly decreases along the rod and then falls to the asymptotic value *Mx* when we approach the extremities. Figure 5-3 shows that the equivalent moment tends at any time to *Mx* at the extremities (for $\eta=1.5mm$, $Mx=0.083Nm$)

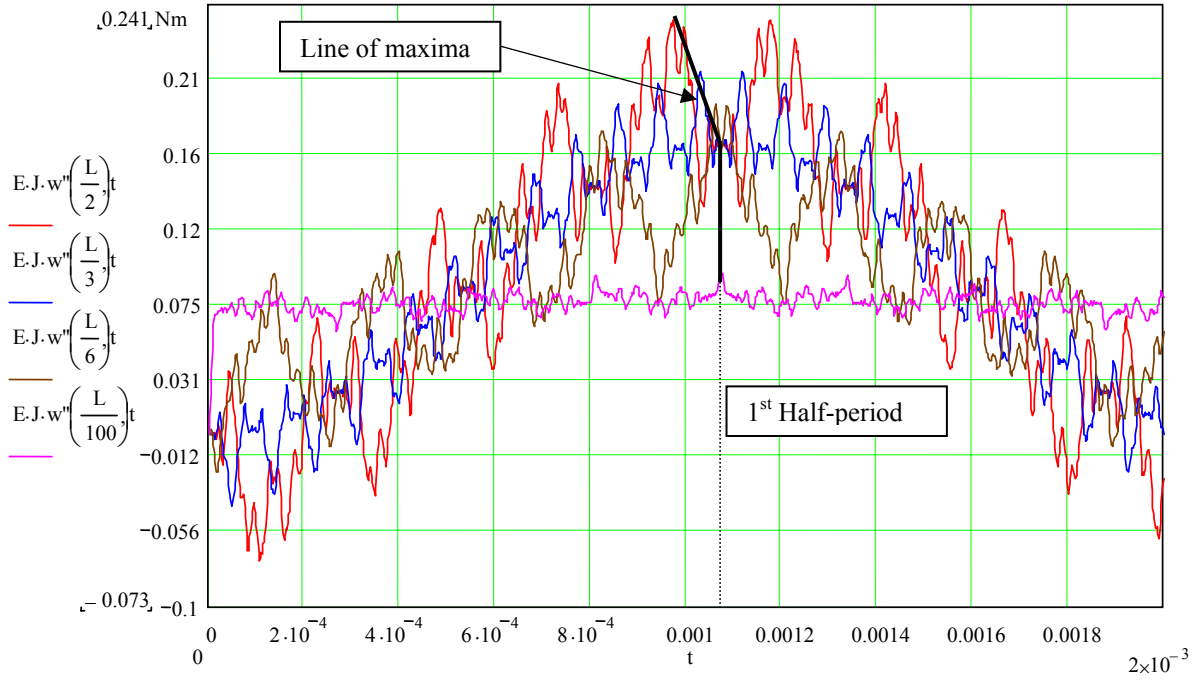

Figure 5-4 Equivalent bending moment at various locations as a function of time

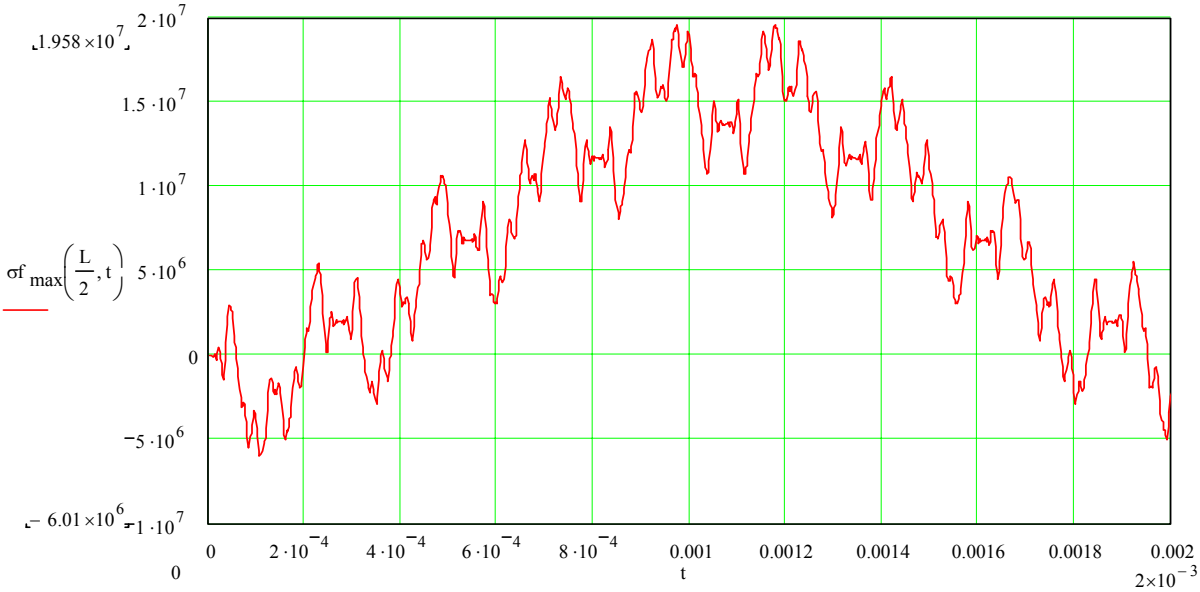

Figure 5-5 Maximum bending stress at mid rod (r=R; θ=3π/2) (η=1.5mm)

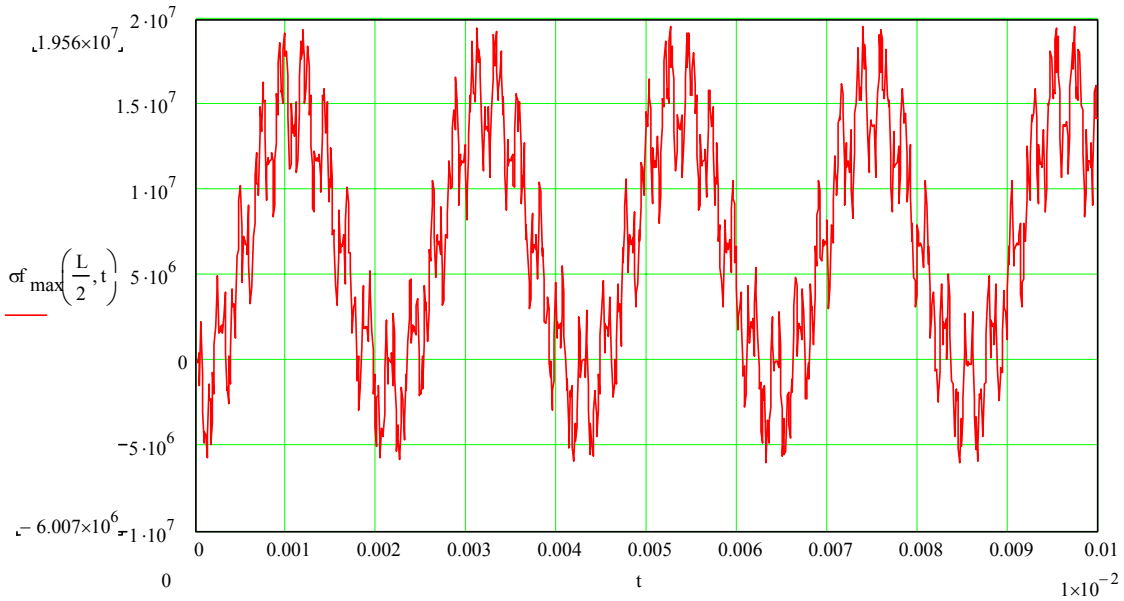

Figure 5-6 Maximum bending stress at mid rod (compressed time scale) (η=1.5mm)

5.3 Longitudinal modal analysis

The longitudinal dynamic stress is calculated with the same method used for dynamic bending. In this case the variable of interest is the longitudinal displacement, which is given by:

(28) $$u_z(z,t) = \sum_i \phi_{zi}(z) \cdot q_{zi}(t)$$

The generalized forces are given by:

(29) $$\frac{Qz_i(t)}{M_i} = \frac{Fz(t_{sp})\sqrt{2}}{M}\left[1-(-1)^i\right]\cdot g(t) = Fz_i \cdot g(t)$$

Natural modes and natural frequencies are:

(30) $$\phi_{zi}(z) = \sqrt{2}\cos\left(\frac{i\pi z}{L}\right)$$

(31) $$\omega z_i = \frac{i\pi}{L}\sqrt{\frac{E}{\rho}}$$

The parameters of the fundamental harmonic are:

$$\frac{\omega_{z1}}{2\pi} = 11910 Hz$$

$$T_{z1} = 8.399 \cdot 10^{-5}\, s$$

We immediately see that the time scale for longitudinal waves is almost by two orders of magnitude smaller than that of bending oscillations.

Finally, the dynamic longitudinal stress component is calculated as:

(32) $$\sigma_{zDyn}(z,t) = E \cdot u'_z(z,t)$$

where $u'_z(z,t)$ denotes the first derivative of u_z, i.e. the longitudinal strain.

Results are given in the following graphs. From Figure 5-8 we see that the calculated longitudinal stress perfectly matches the result obtained for the axisymmetric case, making use of the finite difference method. For η=*1.5mm*, maximum longitudinal stress is 6.1MPa, which, as found for the axisymmetric case, corresponds to $2\frac{Fz}{\pi R^2}$, i.e. twice the quasi-static longitudinal stress. The dynamic longitudinal stress oscillates between 0 and $2\frac{Fz}{\pi R^2}$, with the quasi-static stress as mean value.

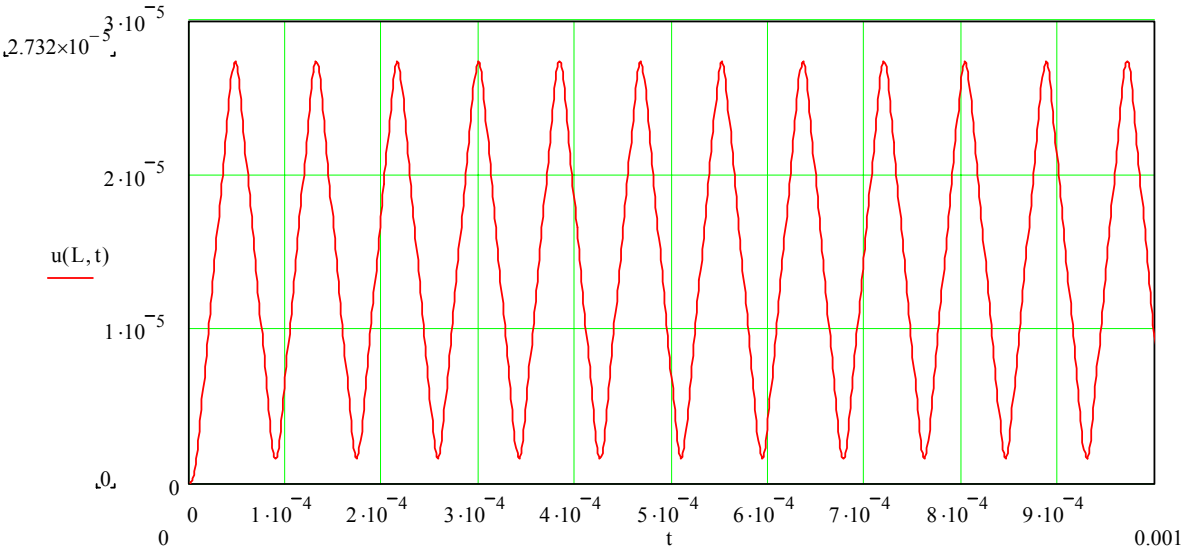

Figure 5-7 Longitudinal displacement at the rod extremities (η=1.5mm)

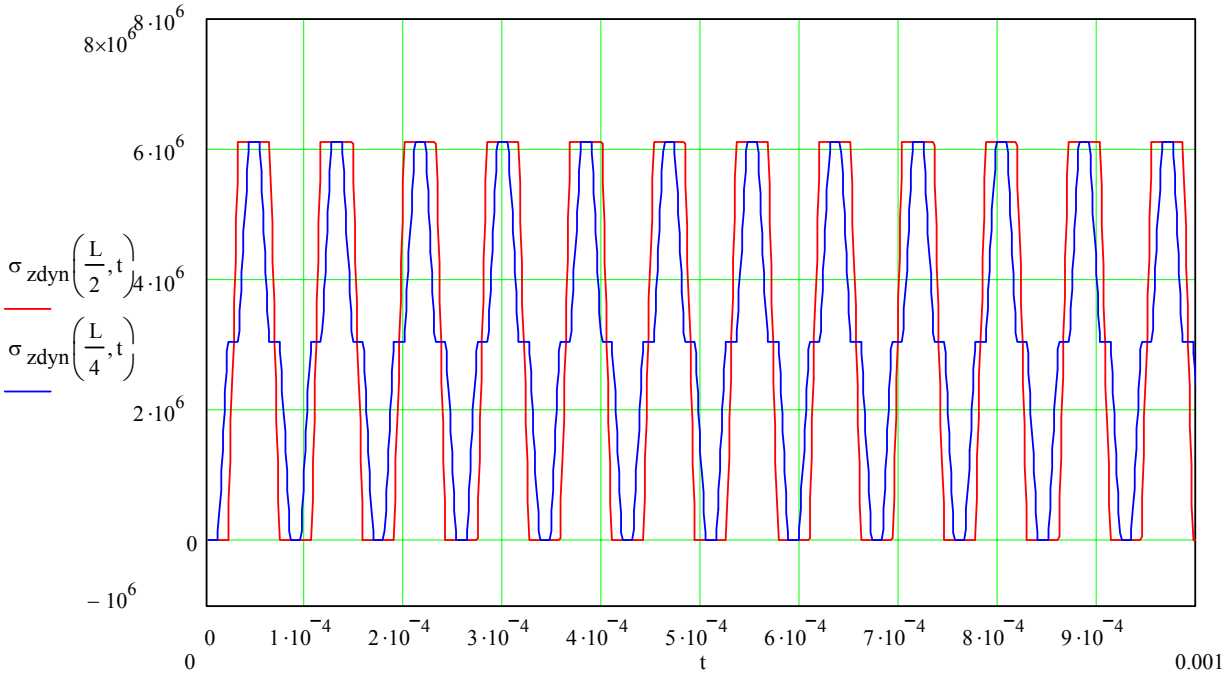

Figure 5-8 Longitudinal stress at mid-rod and L/4 as a function of time (η=1.5mm)

5.4 Equivalent global stress

All the elements are now on hand to calculate the global components of stress acting on the target rods[7]

The global axial stress σ_z is obtained by superimposing the zero-strain quasi-static component (17)(iv) with the dynamic bending stress (27) and the dynamic longitudinal stress (32).

$$\sigma_z(r,\theta,z,t) = \overline{\sigma_{z0}}(r,\theta,t) + \sigma f_{zDyn}(r,\theta,z,t) + \sigma_{zDyn}(z,t) \tag{33}$$

The four global components of stress are given by eqs. (17)(i), (ii), (iii) and (33).

To assess the structural risk for the rods, we must choose a Criterion of elastic failure leading to the calculation of an equivalent tensile stress. Among the many available methods, the one best coping with the non-symmetric elastic behavior in tension and compression of the graphite seems to be the **Stassi-d'Alia** criterion. For our four-component state of stress, the expression of the equivalent stress is given by:

$$\sigma_{eq} = \frac{(\mu-1)(\sigma_r+\sigma_\theta+\sigma_z)}{2\mu} + \frac{\sqrt{(\mu+1)^2\left[{\sigma_r}^2+{\sigma_\theta}^2+2{\tau_{r\theta}}^2+{\sigma_z}^2+2\left(\mu^2-4\mu+1\right)\left(\sigma_r\sigma_\theta-{\tau_{r\theta}}^2+\sigma_\theta\sigma_z+\sigma_z\sigma_r\right)\right]}}{2\mu}$$

where $\mu=3.3$ is the ratio between the compressive and tensile elastic limit of graphite.

We are particularly interested to the absolute maximum of the function $\sigma_{eq}(r,\theta,z,t)$ which varies in time and in space. The point and the instant at which σ_{eq} is maximum cannot be known a priori. Anyhow, considering that quasi-static stresses (17)(i), (ii), (iii) are constant along the axis, while longitudinal dynamic stress (32), though not constant with z, takes on everywhere the same maximum value (Figure 5-8), we come to the conclusion that the most loaded section is the mid-rod section where dynamic bending stress is maximum (Figure 5-4).

Furthermore, bearing in mind that all quasi-static components decrease with time as temperature, the maximum in time must be found either at t_{sp} (when quasi-static stresses are highest) or at t_{f1} (when bending moment reaches first peak): a rapid check allows to verify that maximum is found at t_{f1}. If we graphically check mid-rod section at time t_{f1}, we see that the most loaded point is found at $r=R$, $\theta=3\pi/2$, i.e. on the section boundary, in the direction of eccentricity. The value of tension here only depends upon σ_θ and σ_z, since on the surface the other components of stress are zero.

We report in Figure 5-9 the equivalent stress for most loaded point as a function of time when $\eta=1.5mm$. The peak reached at time t_{f1} can be very well appreciated: its value is $25.3MPa$, while $t_{f1}=0.973ms$.

If we change eccentricity, it is very interesting to note that maximum equivalent Stassi stress is found for $\eta=1.23mm$. This result, which might look unexpected, is due to the fact that axial stress reaches a maximum for $\eta\approx1.1mm$ and then starts to decrease. Tangential stress continues to increase with eccentricity, but its effect is completely offset by diminishing axial

[7] As mentioned above, this is strictly true in the hypothesis of confounding the global radial and tangential stress with their quasi-static values.

stress (Figure 5-10), so producing a maximum for equivalent Stassi stress. Highest equivalent stress at $\eta=1.23mm$ is $27.1MPa$.

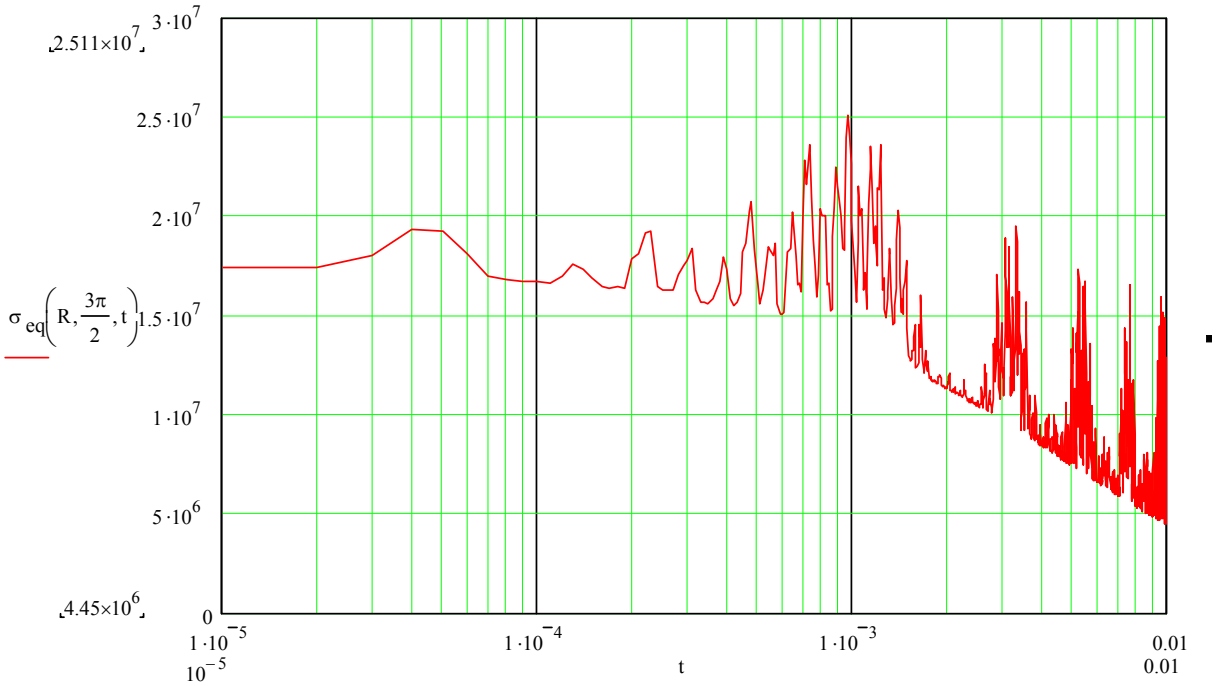

Figure 5-9 Equivalent Stassi stress at r=R, θ=3π/2 as a function of time (η=1.5mm)

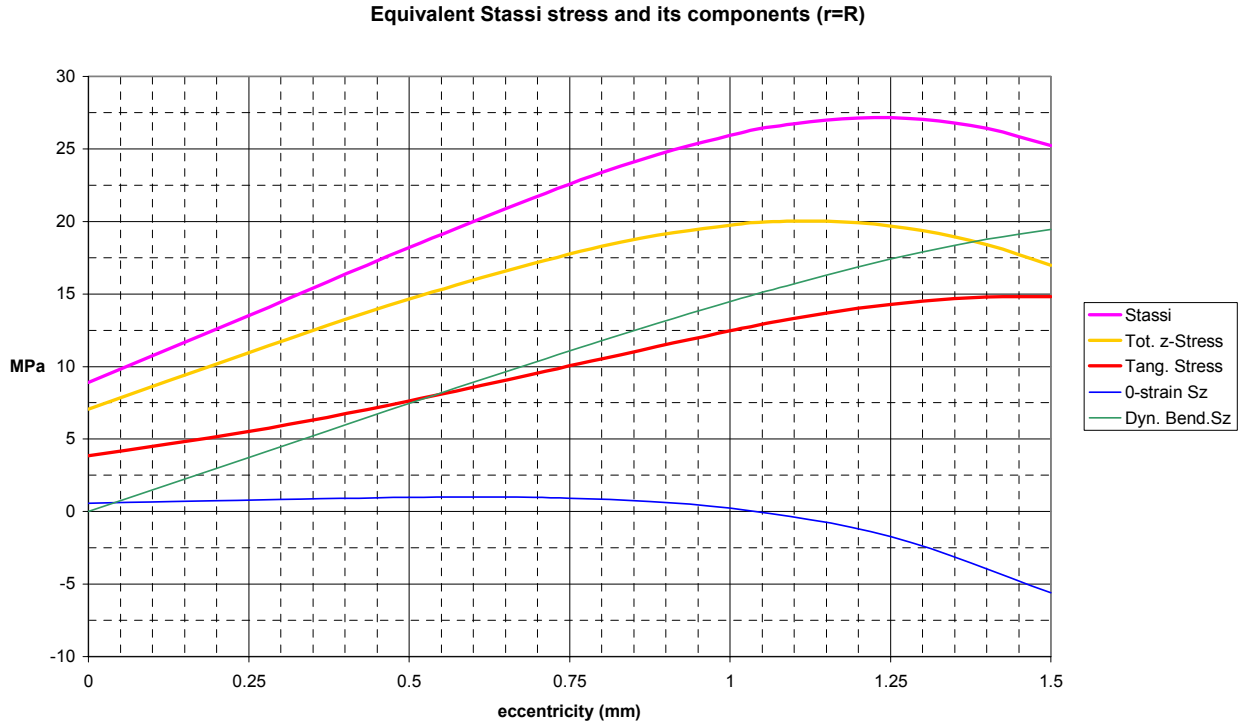

Figure 5-10 Equivalent Stassi stress and components as a function of eccentricity

5.5 Effect of successive bursts

As mentioned at the end of thermal analysis, when the second proton burst hits the target thermal equilibrium has not been reached yet (see Figure 5-11). Subsequently, also quasi-static stresses, which depend upon temperature gradient, are non-zero. This means that that stresses induced by the second burst sum up with the remnant stresses of previous burst.

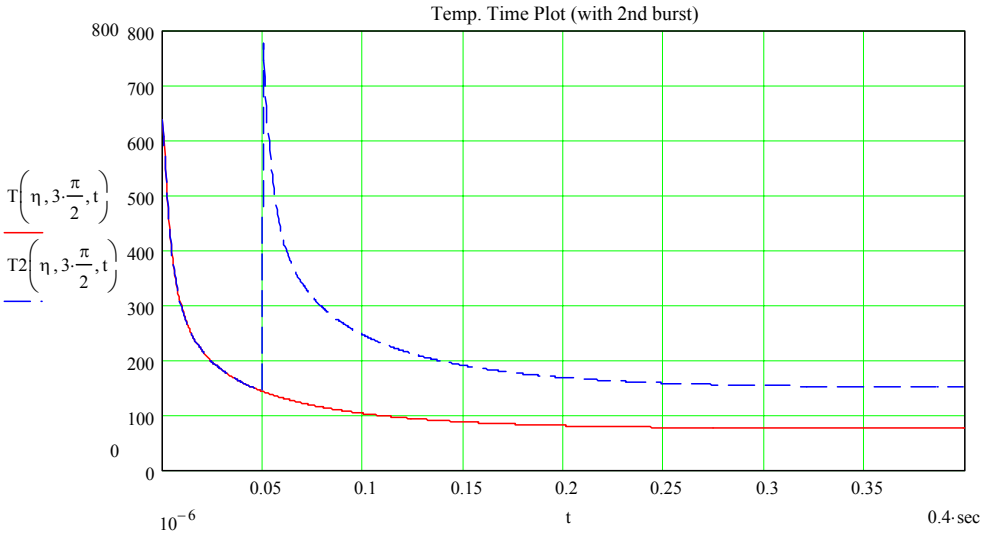

Figure 5-11 Temperature as a function of time for a single and double burst (η=1.5mm)

Since the system is supposed linear, the principle of superposition still holds[8]. Thus we may obtain new stress state by simply by simply adding to terms like *f(t)*, functions like $f(t-t_b)$, where t_b is the time elapsed between two successive bursts (*50ms*). This method has a major drawback: the assumption made for the "equivalent" bending moment no longer holds, since upon time t_b, M_x is no more constant as initially assumed (see par. 5.2). This hurdle can be overcome by assuming a linear decay of M_x over the time up t_b, hence better interpolating real behaviour (Figure 5-12).

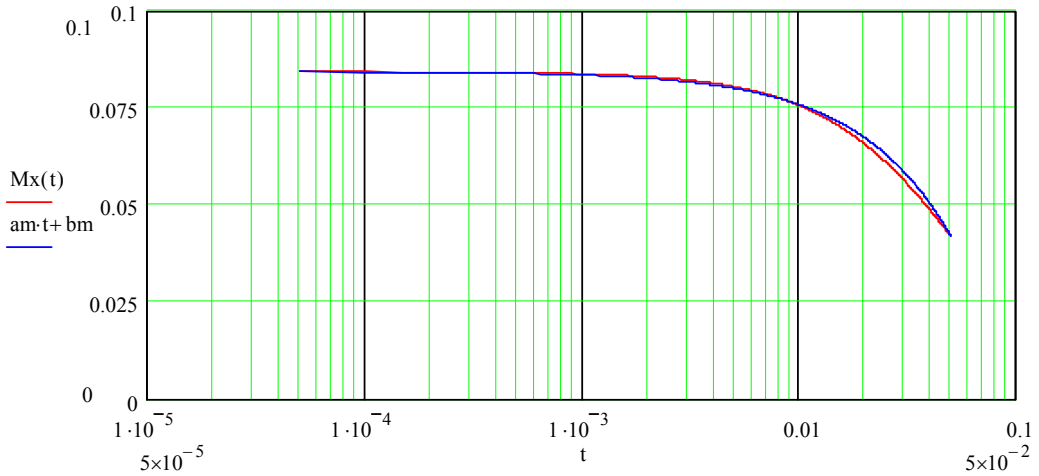

Figure 5-12 Comparison between actual bending moment and linear interpolation (log plot)

[8] We assume here that the second burst hits the target in its rest position. In reality, at instant of proton beam impact, displacement may be non-zero (see Figure 5-2), thus, the rod could be bent under the effect of equivalent moment: this deformation would modify the eccentricity of the proton beam. Since the lateral displacement is always in the direction of the eccentricity, "apparent" offset would be reduced. Assuming a straight rod means that we maximize the effects of second burst.

The function *g(t)* of Figure 5-1, is now replaced by another excitation *g'(t)*, combination of two ramp functions as shown in Figure 5-13

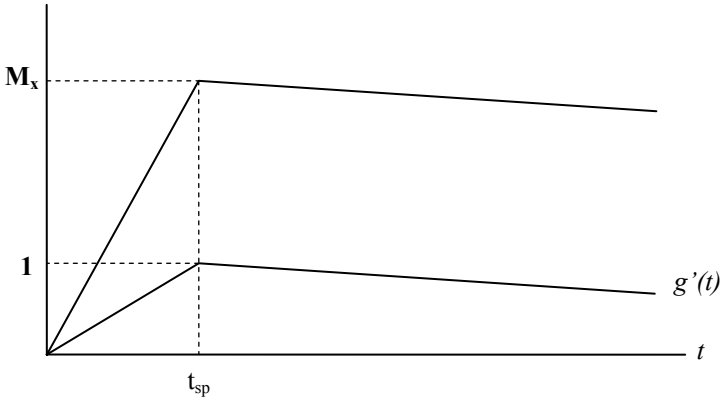

Figure 5-13 Equivalent excitation for Bending moment with linear decay

Mode shapes and natural frequencies remain the same previously calculated. The solution for this case can be obtained by superimposing the response to two ramp functions offset in time.

In line with what assumed in chapter 5, results do not change up to the first milliseconds. On the contrary differences arise from then on, as shown in Figure 5-14 and Figure 5-15 (compare with Figure 5-2 and Figure 5-6).

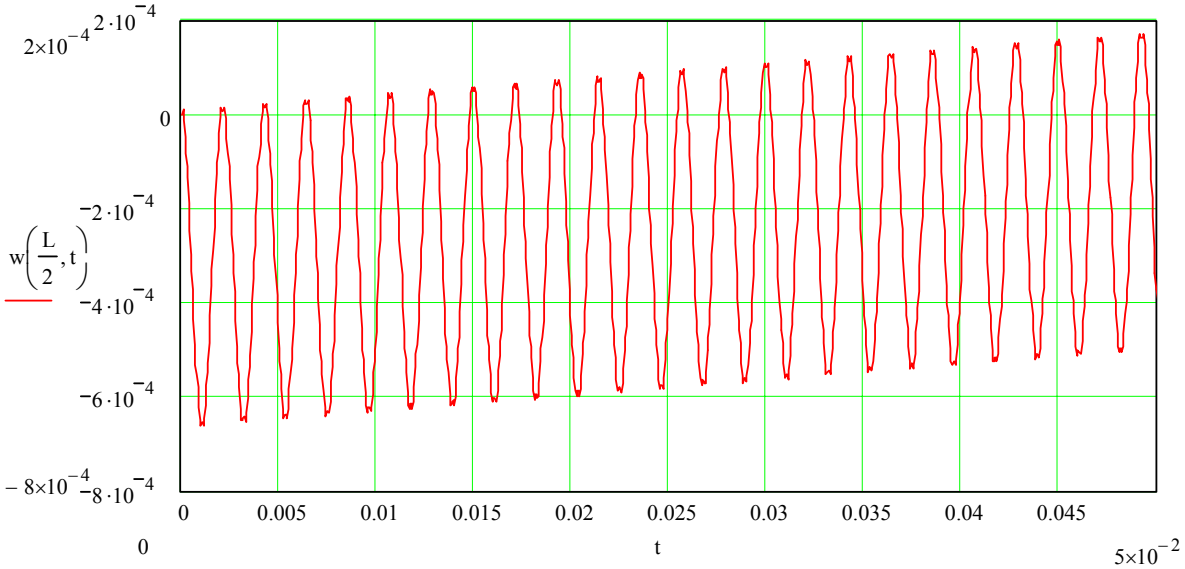

Figure 5-14 Lateral displacement at mid rod assuming linear decay for Mx (η=1.5mm)

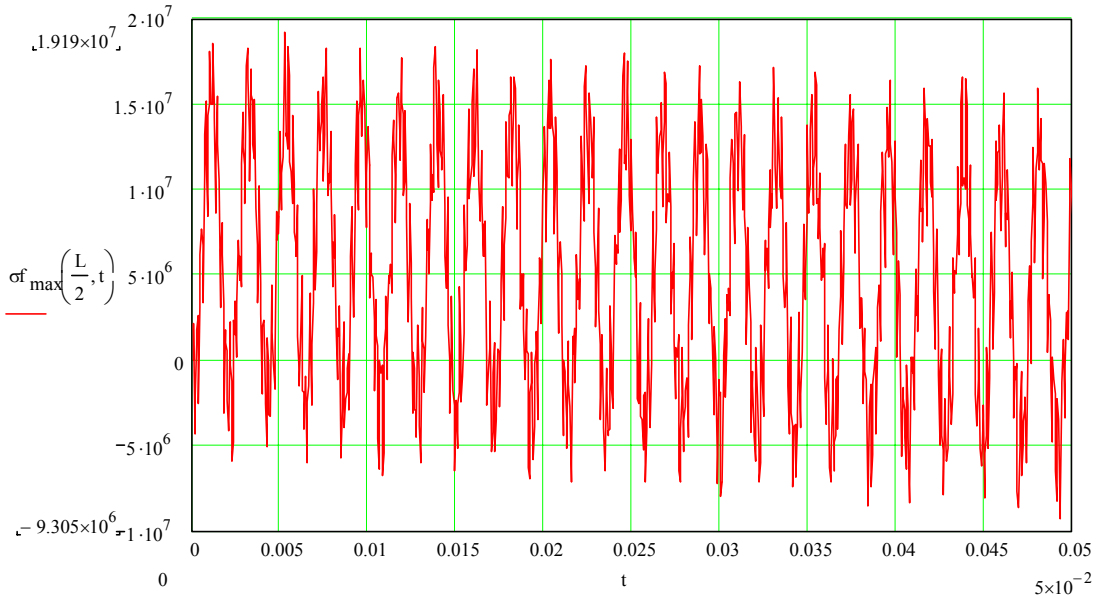

Figure 5-15 Maximum bending stress at mid rod (r=R; θ=3π/2) assuming linear decay for Mx (η=1.5mm)

With a more accurate solution for dynamic bending stresses, we can now recompute equivalent stress, induced also by a second burst, as announced above.

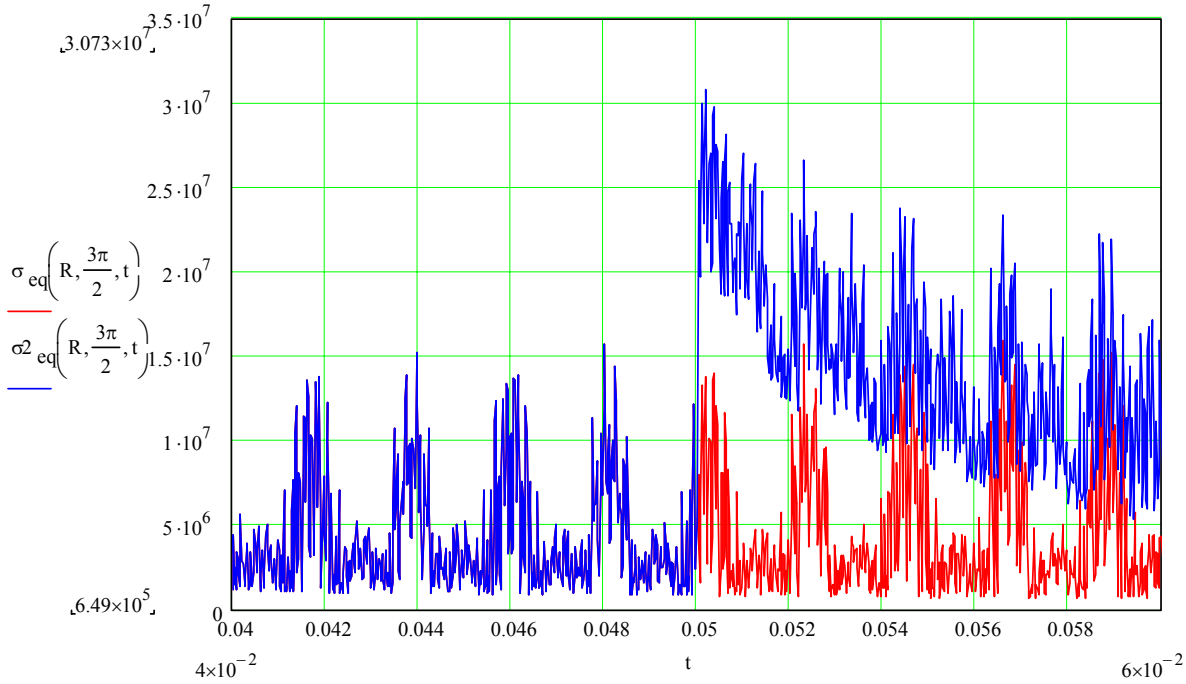

Figure 5-16 Equivalent Stassi-stress for single and double burst (η=1.5mm)

As we may see from Figure 5-16, new maximum is reached after the second burst, at *t=0.05037s* with a peak of ***32.4MPa***, i.e. roughly *7MPa* more than top stress after the first pulse. The increase in maximum equivalent stress tends to reduce with smaller eccentricities, as we may see from Figure 5-17; for *η=1.2mm* this difference reduces to *4.1MPa*.

If we were to continue our analysis, still worse cases could be expected for successive bursts, with maximum equivalent stress continuing to build up. However we must remember that the hypothesis of adiabatism was initially made in the assumption of a short time-scale. If

time-scale is enlarged, adiabatism no longer holds since phenomena of heat radiation and forced convection must be taken into account.

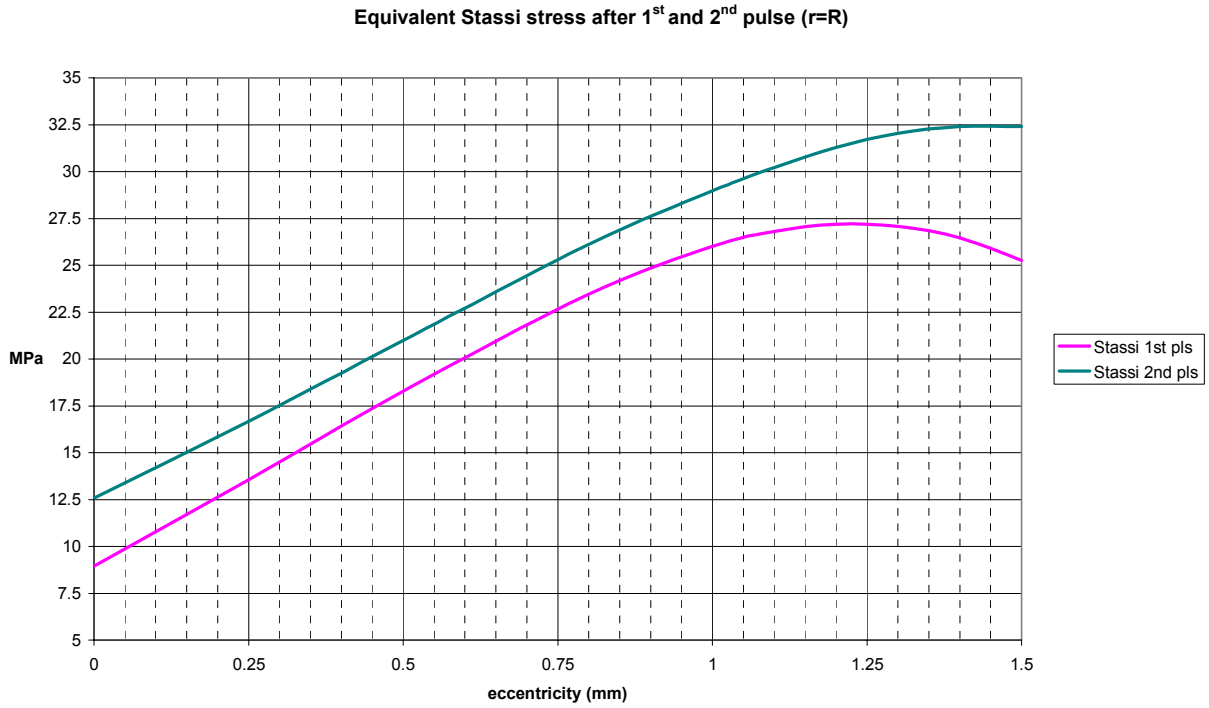

Figure 5-17 Maximum Stassi stress at r=R, $\theta=3\pi/2$ after first and second burst as a function of eccentricity

6. CONCLUSIONS

In this note, a model to study the influence of a sudden heating with off-axis Gaussian distribution, induced by a fast extracted proton beam, over a cylindrical rod was developed. The problem was solved using analytical methods, with constant, mean values for thermodynamic and mechanical material properties, assuming adiabatic boundary conditions.

The temperature distribution was first calculated as a function of time and space, with the initial conditions expanded in a Fourier-series. The results lead to some important conclusions:

1. The time necessary to reach thermal equilibrium increases with eccentricity, changing from *0.093s* for the axisymmetric distribution to *0.364s* for 1.5mm-eccentricity. This automatically implies that the effects of one burst have not vanished yet when the next one hits the target.
2. As one could expect, final temperature is lower for higher eccentricities, since deposited energy is less, as part of the proton beam "misses" the target. For $\eta=0$, $Tf=81ºC$; for $\eta=1.5mm$, $Tf=74.7ºC$.

Once known the temperature distribution, quasi-static stresses were calculated making use of the General theory of elasticity in the assumption of plane-strain behaviour (long cylinder). Quasi-static stresses were obtained by superposition of two parts: the first satisfying the thermoelastic equation, the latter restoring free-boundary condition. To ensure axial equilibrium equivalent axial force and bending moment were then added. The quasi-static stresses so calculated, constant along the rod axis, depend upon the eccentricity.

In general, if Stassi-d'Alia criterion is applied, maximum quasi-static equivalent stress is found on the outer surface, aligned with the radial direction of maximum eccentricity for offsets larger than 0.6mm, while for smaller eccentricities, highest equivalent stress moves towards the heat centre ($r=\eta$). Its value roughly increases with eccentricity, form *14MPa* for $\eta=0$, up to *20.2* for $\eta=1.5mm$.

To take into account the dynamical effects, which were neglected in the quasi-static analysis, a dynamic model was developed. This model led to the calculation of longitudinal dynamic stresses, while for the other component of stress it has been seen that they could be confounded with their quasi-static value. The dynamic component in the axial stress was due to the sudden application of the axial force and the bending moment arising to ensure axial equilibrium, which generate longitudinal waves and lateral oscillations respectively.

The dynamic analysis saw an increase in the equivalent Stassi stresses with respect to quasi-static analysis; in particular it was noticed that:

1. The fundamental harmonic of the transverse oscillations has a frequency of *467Hz* corresponding to a period of *2.139e-3sec*. First stress peak is reached at about $tf1 \approx 1ms$
2. the fundamental harmonic of the longitudinal waves has a frequency of *11910Hz* corresponding to a period of *8.399e-5 sec*
3. Maximum equivalent Stassi stress takes place at *t=9.73e-4s*, when the first peak of the bending moment is reached.
4. Maximum equivalent Stassi stress is found for $\eta=1.23mm$ and is 27.1MPa. This result, which might sound unexpected, is due to the fact that axial stress reaches a maximum and then starts to decrease. Tangential stress continues to increase with eccentricity, but its effect is completely offset by diminishing axial stress, producing a maximum for equivalent Stassi stress. For $\eta=1.5m$ maximum stress is *25.3MPa*.

Finally, considering that the effects of one burst interact with those of the following one, it was calculated the equivalent stress in case of two successive bursts: its maximum is found immediately after the second burst and is the order of *32.4MPa* for $\eta=1.5m$, i.e. as much as 7MPa more, even if this difference decreases with smaller eccentricities.

It is logical to expect a further increase should other impacts take place, but one must bear in mind that over long time scales deposited energy starts to be dissipated by convection and radiation phenomena, therefore calculated stress would be overestimated.

REFERENCES

[1] H.S. Carslaw, J.C. Jaeger, *Conduction of heat in solids*, Oxford University Press, Oxford, 1959

[2] S. Timoshenko, J.N. Goodier, *Theory of Elasticity*, 3rd ed., McGraw-Hill Book Company, New York, 1970

[3] B.A. Boley, J.H. Weiner, *Theory of Thermal Stresses*, John Wiley and Sons, New York, 1960

[4] W.T. Thomson, *Theory of Vibration with Applications,* Chapman & Hall, London, 1993

[5] P. Sievers, *Elastic stress waves in matter due to rapid heating by an intense High-energy particle beam*, CERN Technical Note, Lab. II/BT/74-2, 1974

[6] H. Bargmann, *Dynamic response of external targets under thermal shock*, CERN Technical Note, Lab. II/BT/Int/73-3, 1973

[7] A. Bertarelli, *Analytical study of axisymmetric transient thermal stresses in Graphite Target Rods for the CNGS facility*, CERN EST-ME Technical Note 2003-005, EDMS383454, 2003

[8] T. Mura, *Dynamical Thermal Stresses Due to Thermal Shocks*, Research Reports of the Faculty of Engineering, Meiji University, No. 8, 1956 (2)

[9] K.F. Graff, *Wave motion in elastic solids,* Oxford University Press, London, 1975

[10] J.D. Achenbach, *Wave propagation in elastic solids,* North Holland publishing co,, Amsterdam, London, 1973

Distribution List